



Article

Demonstration of Focusing Wolter Mirrors for Neutron Phase and Magnetic Imaging

Daniel S. Hussey^{1,*}, Han Wen², Huarui Wu³, Thomas R. Gentile¹, Wangchun Chen^{4,5},
David L. Jacobson¹, Jacob M. LaManna¹  and Boris Khaykovich⁶ 

¹ Physical Measurement Laboratory, NIST, Gaithersburg, MD 20899-8461, USA; thomas.gentile@nist.gov (T.R.G.); david.jacobson@nist.gov (D.L.J.); jacob.lamanna@nist.gov (J.M.L.)

² National Heart Lung Blood Institute, National Institute of Health, Bethesda, MD 20892, USA; wenh@nhlbi.nih.gov

³ Key Laboratory of Particle & Radiation Imaging, Tsinghua University, Ministry of Education, Beijing 100084, China; huarui92@163.com

⁴ NIST Center for Neutron Research, NIST, Gaithersburg, MD 20899, USA; wangchun.chen@nist.gov

⁵ Department of Materials Science Engineering, University of Maryland, College Park, MD 20742, USA

⁶ Nuclear Reactor Laboratory, Massachusetts Institute of Technology, Cambridge, MA 02139, USA; bkh@mit.edu

* Correspondence: daniel.hussey@nist.gov; Tel.: +1-301-975-6465

Received: 1 November 2017; Accepted: 2 March 2018; Published: 6 March 2018

Abstract: Image-forming focusing mirrors were employed to demonstrate their applicability to two different modalities of neutron imaging, phase imaging with a far-field interferometer, and magnetic-field imaging through the manipulation of the neutron beam polarization. For the magnetic imaging, the rotation of the neutron polarization in the magnetic field was measured by placing a solenoid at the focus of the mirrors. The beam was polarized upstream of the solenoid, while the spin analyzer was situated between the solenoid and the mirrors. Such a polarized neutron microscope provides a path toward considerably improved spatial resolution in neutron imaging of magnetic materials. For the phase imaging, we show that the focusing mirrors preserve the beam coherence and the path-length differences that give rise to the far-field moiré pattern. We demonstrated that the visibility of the moiré pattern is modified by small angle scattering from a highly porous foam. This experiment demonstrates the feasibility of using Wolter optics to significantly improve the spatial resolution of the far-field interferometer.

Keywords: neutron imaging; Wolter optics; polarized neutron imaging; far-field interferometer

1. Introduction

Nearly all existing neutron-imaging instruments can be described as pinhole cameras that measure the neutron shadow of a sample. In such cameras, the geometric blur, which fundamentally limits spatial resolution, is given by $\lambda_g = z D / (L - z)$, where z is the sample to detector distance, D is the beam defining aperture, and L is the aperture to detector distance. Due to the inherent low intensity of neutron sources, D is of order 1 cm. This size limitation precludes the use of geometric magnification to improve spatial resolution, and currently achievable spatial resolutions reach $\sim 10 \mu\text{m}$. The primary reason for the utilization of the pinhole geometry is the lack of a practical neutron-image forming lens. While refractive neutron lenses have been incorporated into small angle neutron scattering instruments, they are not suitable for imaging, since the refractive index for materials is $n \sim 1 - 10^{-4} \lambda \text{ (nm)}^2$. Therefore, neutron refractive lenses have very long focal lengths ($\sim 10^7$'s of meters) and are strongly chromatic [1].

The geometric blur limits the achievable spatial resolution especially for methods that require placing of sample environments or optical components between the sample and the detector. We

consider below two examples of emerging techniques which require such equipment: polarized and grating-interferometry imaging. First, after the work of Kardjilov et al. [2], there is renewed interest in exploiting the spin of the neutron to image magnetic fields, for instance the trapped flux in superconductors [3]. In order to measure the magnetic field, one must measure the neutron spin rotation angle by the sample with the help of spin analyzers such as compact polarizing supermirrors or ³He neutron spin filters. These devices require a minimum of $z \sim 20$ cm of separation between the sample and the detector, limiting achievable spatial resolution. The state-of-the-art polarized neutron imaging instrument PONTO [4] has been able to achieve only 120 μm resolution, almost a factor of ten more coarse than what can be routinely achieved using conventional neutron-imaging layouts. Second, the recently introduced broadband far field interferometer is a potentially groundbreaking method of obtaining phase gradient and dark-field images [5,6]. However, in order to probe the longest autocorrelation lengths, one places the sample in the middle of the flight path for a geometric magnification of 2, producing strongly blurred images. While a small aperture could be used to obtain resolution of order 0.5 mm, the strong reduction in intensity would obviate the advantages of the method.

It was recently demonstrated that Wolter mirrors, which are widely used in X-ray telescopes, could be used as neutron-image forming optics [7,8]. Briefly, Wolter mirrors are axisymmetric mirrors composed of two conic sections, see Figure 1. With such optics, one could realize several improvements in neutron imaging over the pinhole optics geometry. First, there is a large distance, of order meters, between the sample and optics (and optics and detector) enabling the introduction of bulky sample environment or beam conditioning devices without the loss of spatial resolution. Second, the image resolution is determined by the optics and not the beam collimation (or L/D ratio). (This is generally true for any optical system which employs image-forming mirrors or lenses.) Therefore, the aperture size D could be increased so that the sample is illuminated by the full power of the divergent polychromatic neutron beam. Third, many mirrors can be nested to increase the solid angle portion of the beam collected by the optics, resulting in orders of magnitude increase in the neutron fluence rate for high spatial resolution imaging. Fourth, optical magnification can be achieved in order to improve the spatial resolution. As in geometrical optics, the magnification is given by the ratio of focal lengths (f_i and f_o in Figure 1).

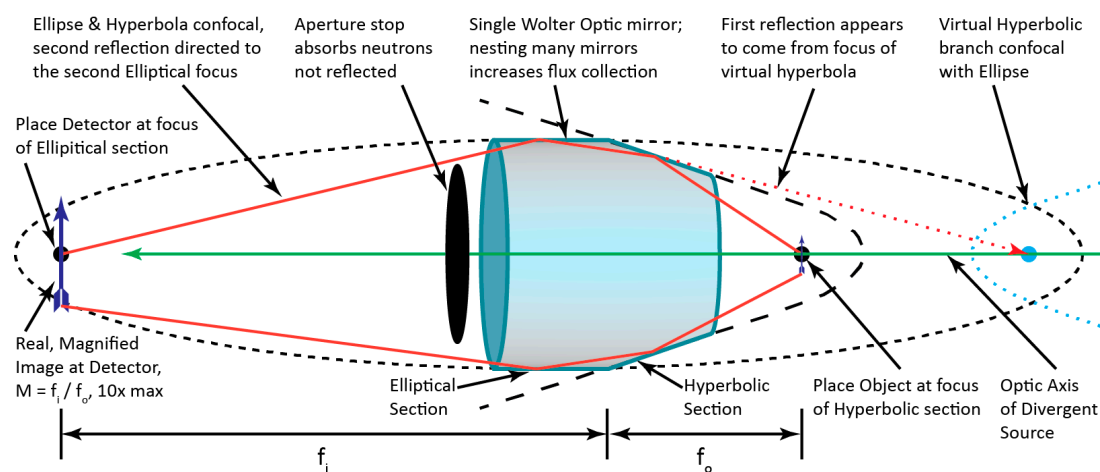


Figure 1. Schematic diagram of a Wolter type I optic composed of a confocal hyperboloid and ellipsoid.

In this article, we demonstrate how to exploit the advantages offered by Wolter optics to polarized imaging, which we refer to as Wolter optics, Helium-3 Neutron imaging of Magnetic Samples (WHIMS), and Wolter Optics Far-Field Interferometry (WOOFF). Specifically, the sample-to-detector separation enables high-resolution, WHIMS, while the image-forming ability of Wolter mirrors enables high-resolution broadband far-field phase imaging [5,6].

2. Materials and Methods

All measurements were made at the cold neutron imaging instrument (CNII) located at the end of the NG6 neutron guide at the NIST Center for Neutron Research [9]. The neutron imaging detector consisted of a 150 μm thick LiF:ZnS scintillator screen viewed by an Andor NEO sCMOS (Andor Technology: Belfast, Ireland) detector [10] through a Nikon 50 mm f/1.2 lens via a mirror at 45 degrees to place the camera out of the gamma and fast neutron beams from the direct line of sight to the reactor core. With this configuration, the effective pixel pitch is 51.35 μm with a field of view of about 13 cm \times 11 cm and a spatial resolution of about 150 μm .

2.1. Wolter Optic

The Wolter optic employed in these measurements consisted of 3 nested nickel mirrors composed of a hyperbolic and an elliptical section with focal lengths of 0.64 m and 2.56 m for an overall focal length $F = 3.2$ m, a magnification of 4. The mirror diameters were about 3 cm and the overall length was about 6 cm, as described in detail elsewhere [7,8]. The angular resolution of about 110 μrad , coupled with the focal length of 0.64 m result in an image spatial resolution of about 100 μm . Aperture stops and diaphragms were placed both upstream and downstream of the optic to block the direct, unfocused beam. In both experiments, the optic was used in magnification mode, so that the optic to sample distance was 0.64 m. The optic was aligned in pitch and yaw by observing when an image of a 1.6 mm diameter hole placed at the focal position ($f_0 = 0.64$ m) was well formed.

The small optic was manufactured for test and validation purposes, not to maximize the intensity and resolution at CNII. Therefore, the signal rate was relatively small. Also, a reduction of the intensity in the center of the image was observed, indicating under-illuminated optics due to insufficient divergence of the neutron beam passing through the sample. With the far-field setup, the field of view was offset from the optical axis by about 2 cm. As a result, the usable portion of the focused image is limited. In the discussion section, we comment about the possibility for future improvements.

2.2. Wolter Optics, Helium-3 Neutron Imaging of Magnetic Samples (WHIMS)

The layout of the experiment and a photograph of the WHIMS setup are shown in Figure 2. The sample was a solenoid, which had a rectangular cross section and was aligned so that the short face of the rectangle was perpendicular to the beam. The solenoid's cross-section is about 15 mm \times 7 mm with rounded corners and has a winding density of 2200 m^{-1} of aluminum wire. A Hall probe was used to determine the magnetic field for a given current setting. The field was linearly proportional to the current; at 0.4 A, a field of 1.5 mT was measured. In this case, a near uniform spin rotation of the polarized neutrons passing through the solenoid field results in a decrease in the observed transmission through the analyzer for a given magnetic field. For $B = 1.5$ mT and $\lambda = 0.6$ nm, a spin rotation of about 2π is expected through the long direction of the solenoid cross-section, which corresponds to a maximum in transmission, while the minimum transmission occurs when the spin is rotated by π at half that field, for $I = 0.2$ A.

A double monochromator composed of two 5 cm \times 5 cm highly oriented pyrolytic graphite (HOPG) (002) crystals was positioned to select a neutron wavelength of 0.6 nm. The neutron wavelength resolution of $\delta\lambda/\lambda \sim 1\%$ from the monochromator was finer than required to connect the observed spin rotation to the magnetic field within the solenoid [2], and it would be possible to perform measurements with coarser wavelength resolution, for instance using a velocity selector with $\delta\lambda/\lambda \sim 10\%$ which would increase the time resolution.

There are two primary techniques for spin-polarizing a neutron beam, polarizing supermirrors or dense samples of hyperpolarized ^3He . The advantages of ^3He include the ability to polarize a divergent beam while introducing no additional structure into the open beam image. For these experiments, two neutron spin filters of ^3He contained in glass cells were polarized via spin exchange optical pumping (SEOP) [11,12]. The first cell, denoted by the name Francis, polarized the beam. It was 9 cm in diameter

with entrance and exit windows made of silicon. The relaxation time of Francis was $\cong 68$ h, and the initial polarization was $\cong 56\%$. The second cell, Spock, spin-analyzed the beam that transmits through the solenoid. Spock had flat aluminosilicate glass windows, a relaxation time of $\cong 120$ h and an initial polarization of $\cong 62\%$. An issue with the nuclear magnetic resonance system used to invert the ^3He polarization for the first cell delayed the beginning of the measurement time by 24 h for Spock, and did not permit complete polarization of Francis. Despite this, the initial flipping ratio for spin-parallel and spin-antiparallel measurements was $\cong 14$, which was more than sufficient for these demonstration measurements. Measurements were made over a period of 15 h. The flipping ratio decreased over the 15 h measurement to $\cong 8$. We note that NIST is developing systems that will be able to continuously polarize ^3He neutron spin filters via the SEOP method on the beam line so that the flipping ratio will be constant in time.

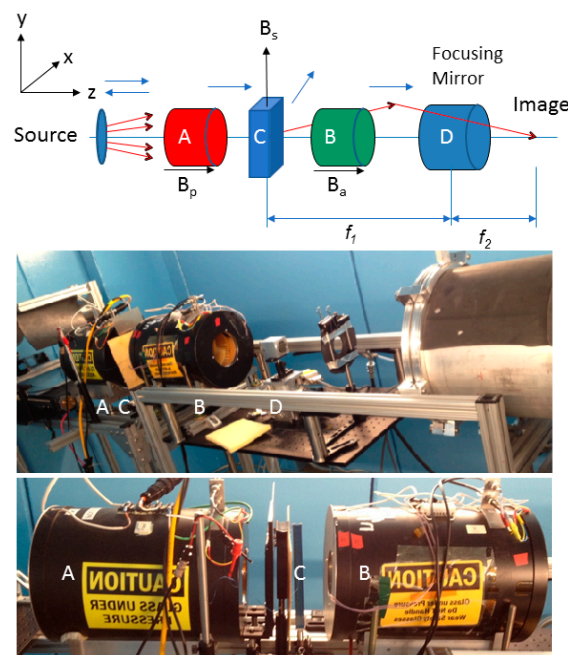


Figure 2. Layout sketch and two photographs of the WHIMS experiment. The beam travels left to right along the positive z -direction. Visible in the top photograph are the ^3He polarizer (labeled with a white A), ^3He analyzer (labeled with a white B), the Wolter optic inside the small aluminum box (labeled with a white D), beam-limiting aperture, and the evacuated beam tube. In the bottom photograph, the polarizer solenoid, the sample solenoid (labeled with a white C) placed in the focal plane of the Wolter optic, and the analyzer solenoid are shown. Due to the use of solenoidal holding fields, the neutron polarization axis, shown as blue arrows in the sketch, is along the z -direction. The longitudinal magnetic fields from the magnetically shielded polarizer and analyzer solenoids drop off rapidly but are sufficient to maintain the neutron’s spin direction. Since they are roughly an order of magnitude lower than that of the sample solenoid’s vertical field, they were not include in the analysis. The sample field, B_s , is along the y -axis, thus causing the neutron spin vector to rotate in the x - z plane. The detector is far beyond the left edge of the photograph.

The count rates for this demonstration experiment were relatively low. The reasons are that the total transmission through the two ^3He cells was about 5% in the spin parallel condition, and the intensity at 0.6 nm is about half that obtained at the peak of the NG6 spectrum. (The 0.6 nm was chosen to suit the critical-reflection-angle requirement for the test Wolter mirrors used for this measurement. Optimization of the mirrors for the beamline spectrum is straightforward and would result in significant increase in the signal intensity.) As a result, the camera was set to 4×4 binning and images were acquired for 120 s; since the optic has magnification 4, the effective pixel pitch remained

51.35 μm . Each magnetic field condition was measured for a minimum of 30 min. To further reduce the noise, 5 images were combined with a boxcar median filter and a stripe filter based on wavelets removed the variation due to readout noise and then the average of the remaining time series was formed (3 images in the case of 30 min total exposure time).

2.3. Wolter Optics Far-Field Interferometry (WOOFF)

Neutron grating interferometry is a collection of new imaging techniques exploring interference phenomena to image spatial distribution of refractive index of samples, the most common interferometer geometry being the Talbot-Lau. A new technique that we explore here is a far-field interferometer, which consists of two phase modulating gratings of period P_g . When illuminated by a wave with sufficient transverse coherence the gratings produce a moiré pattern at the detector with a period which depends only on the geometry of the setup and is independent of wavelength. However, the visibility of the fringes is wavelength dependent. One can use a source grating with period P_s to create the transverse coherence while preserving a high intensity of the neutron beam. The relative positions of source, gratings, Wolter optic, sample and detector are inter-related through the following considerations [7]. The detector, optic and sample positions are fixed by the geometry of the optic. The separation from the source grating to detector, L , is determined by $L = P_s D/P_g$, where D is the separation of the two phase gratings. In order to have transverse coherence at the sample larger than the autocorrelation length, ξ , the gratings are placed downstream of the sample position, z , so that $L = z + F$ and $\xi = \lambda z/P_s$. The period of the moiré pattern at the detector will be enlarged by the magnification of the optic, in this case a magnification of 4.

As with other harmonic imaging methods, if the sample has a dispersion in the microstructure, the visibility of the interference pattern will be reduced [13]. If one can tune the autocorrelation length of the interferometer, ξ , and measure the reduction in the fringe visibility as a function of ξ , one measures the pair distribution function of the sample. This function is connected to the form factor measured in small angle scattering measurements via the Hankel transformation. However, these measurements didn't scan ξ , rather only the thickness of the sample was increased to observe a change in fringe visibility.

For this demonstration, we employed optical components that were readily available, namely the phase modulating gratings had a period of 2.4 μm , the source grating was composed of Gadox powder deposited onto silicon combs with a period of 354 μm and duty cycle of 40%, and the Wolter optic previously described. This led to the configuration, which is shown in Figure 3, and which was expected to produce a moiré pattern with 1.4 mm period and 2% fringe visibility (FV) at the detector. The theoretical limit of the FV with two ideal gratings and a point source is above 50% for a broadband neutron beam. The 2% estimate comes from the 4.5% FV of the earlier 2-grating far field experiments [6], modified by the geometry of the 0.354 mm slit array. Two factors that reduced the FV are 1: the mismatch between the available grating periods (2 gratings of the same 2.4 μm period) and the 0.354 mm slit array period within the geometry of the Wolter lens setup; 2: grating profiles which we knew were not ideal from the earlier FFI experiments [6]. If we purpose-made gratings for the Wolter lens setup, the FV could have been higher by an order of magnitude.

The ability to observe the moiré pattern requires fine angular alignment of the phase gratings (0.001°). The moiré pattern created with a source grating is also only observed for a small range of phase grating separations. In order to facilitate the initial alignment, the gratings of the far-field interferometer were first aligned using a single source slit with a 8.4 m total flight path length, similar to the configuration described previously [8]. Once aligned, the gratings were translated along the rail system of the CNII which maintained their mutual alignment.

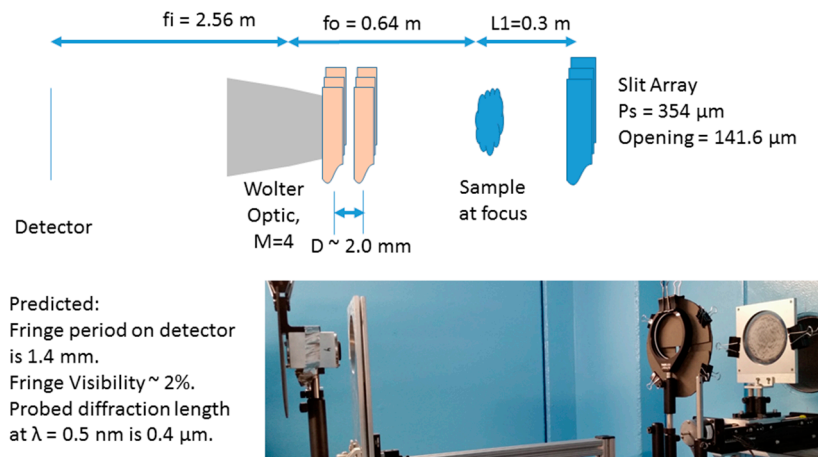


Figure 3. Schematic and photo of the WOOFF experiment. The beam propagates from right to left. The two phase gratings are visible followed by the optics. The detector is beyond the edge of the photograph.

3. Results

3.1. WHIMS

Images of the solenoid at magnetic fields of 0 mT, 0.375 mT, 0.75 mT, 1.125 mT and 1.5 mT were acquired. The images were background corrected, and the states with magnetic field were normalized to that with no field, and these are shown in Figure 4.

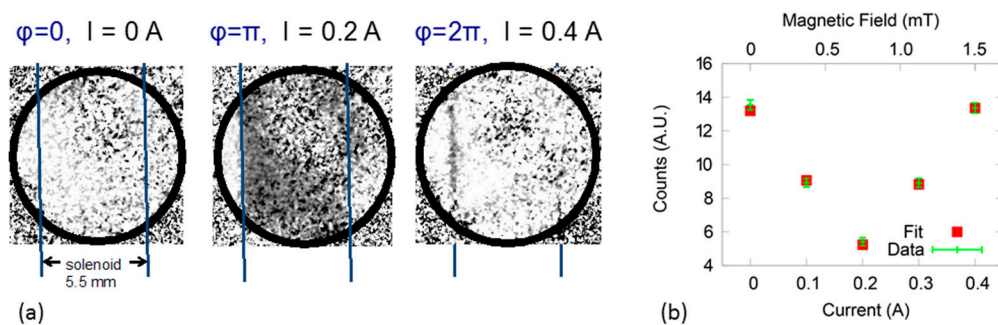


Figure 4. (a) Transmission images of the solenoid at three different applied currents. The reduction of transmission due to neutron spin rotation by the solenoid’s field is apparent. In the three images, the black circle is the boundary of the field of view and the parallel lines show the position of the solenoid. Due to the low number of counts, there is enhanced “salt and pepper” noise. (b) Average grey level value within the solenoid for given applied current and the fit using the cosine function. The uncertainty is the one-sigma root mean square deviation over the solenoid region.

The transmission through the polarizer-solenoid-analyzer system depends on the neutron spin orientation. The spin precession angle φ in the applied field B at the neutron velocity v is

$$\varphi = \omega_L t = \frac{\gamma_L}{v} \int_{path} B ds, \tag{1}$$

where γ_L is the gyromagnetic ratio and neutron Larmor precession frequency ω_L in the magnetic field B . The transmission of the polarized ^3He analyzer strongly depends on the spin state of the neutrons. The attenuation of the polarized beam due to the spin rotation is given by

$$I(x, y) = I_0(x, y) \cdot \frac{1}{2} (1 + \cos \varphi(x, y)) \quad (2)$$

Therefore, the transmission is suppressed when the field corresponds to $\varphi = \pi$, and recovered for $\varphi = 2\pi$.

Figure 4 shows 3 images (a) and integrated intensities (b) as a function of the applied magnetic field. Flat-field images with the beam blocked were subtracted. In the bottom figure, the intensity is integrated over the area of the solenoid and the change in intensity is fitted with the cosine Function (1), taking into account the parameters of both ^3He cells. The two fitting parameters are the period of the oscillation, (0.403 ± 0.006) A, and the background, (4.6 ± 0.1) in arbitrary units, where the uncertainty is the one-sigma root mean square deviation from the least squares fit. Interestingly, at 0.4 A ($\varphi = 2\pi$) the solenoid's boundary is clearly visible as a sharp line. This is due to the neutron trajectories, which cross the solenoid near the corners, and thus their path lengths are shorter than needed to rotate the spin by 2π . Note that the inhomogeneity near the center of the images is due to under-illumination of the mirrors by the collimated beam, as discussed earlier.

In addition, we modeled our experiment in ray-tracing simulations using McStas [14,15], including the polarizer, solenoid, analyzer and Wolter mirrors. The calculated intensity at the detector is a cosine function with the period of 0.4 A, consistent with the measurements, validating the concept of the polarized neutron microscope.

3.2. WOUFF

The measurements were obtained for only one autocorrelation length, $\xi = 0.4 \mu\text{m}$. (Limited beam time did not permit extensive studies of the WOUFF setup.) To determine if the observed moiré pattern was due to the far field interferometer and not merely an image of the source slit, the gratings were removed and the pattern disappeared. Additionally, three thickness of high temperature insulation were placed at the focus of the Wolter optic. The foam is composed of aluminosilicate fibers with diameter $3.5 \mu\text{m}$ and length of about $50 \mu\text{m}$ with a material mass density of 0.1 g/cm^3 and was shown previously to have high transmission, but strong attenuation of the far-field fringe visibility. As is shown in Figure 5, the Wolter optic preserves the coherence of the beam so that the moiré pattern of the open beam is clearly observed and has the expected period, measured to be 1.4 mm. A higher fringe visibility than expected was observed, likely due to the fact that the Wolter optic preferentially focuses longer wavelengths. Further, the foam attenuates the fringe visibility but not the overall intensity indicating that the observed moiré was in fact due to the far-field interferometer and not merely the image of the source slit grating. (The foam destroys the incident beam coherence because of the interference between the incident and forward-scattered beam. Therefore, the fringe visibility also decreases.).

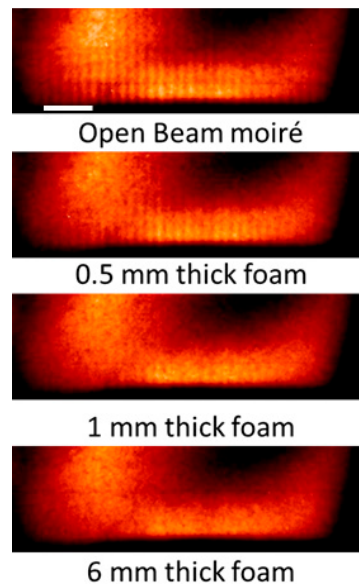


Figure 5. WOOFF images showing the open beam moiré pattern, the reduction in fringe visibility for three thicknesses of insulation, 0.5 mm, 1 mm and 6 mm. The white scale bar in the open beam image is 7 mm.

4. Discussion and Conclusions

We have demonstrated that Wolter optics can be used to obtain high spatial resolution images of the magnetic field distribution. As well, the mirrors are of sufficient quality to preserve the transverse coherence of grating interferometers. The observed count rates were low due to the limited divergence of the beam (about 0.5°), whereas the optimal divergence would be about 1.3° for the mirrors employed here. The reduced divergence also reduces the field of view and introduces non-homogeneities into the open beam image. While the observed spatial resolution of about $100\ \mu\text{m}$ is better than typically observed for polarized neutron imaging, finer spatial resolution would be desired. As a comparison, in polarized imaging, a sample to detector separation of about 50 cm is needed to accommodate the neutron analyzer after the sample, creating a geometric unsharpness on the order of 1 mm. Using the optics employed in this work, it is possible to improve the time resolution and field of view by use a focusing guide (such as a parabolic mirror) to produce the optimal divergence. Further improvements can be realized through design of instrument specific optics. We are pursuing the development of a 1:1 optic which will consist of 10 nested shells ranging in diameter from 10 to 15 cm with a total mirror length of 20 cm with object and image focal lengths of 3.5 m. New mirror fabrication methods are being pursued that are believed will improve the angular resolution of the mirrors from $100\ \mu\text{rad}$ to $5\ \mu\text{rad}$ so that the achievable resolution will be $\sim 20\ \mu\text{m}$ with 3.5 m focal lengths. Ray tracing results indicate that this optic will improve time resolution by about a factor of about 70 with a field of view of at least 1 cm [16]. With such improved optics, the spatial resolution of magnetic imaging and far-field interferometry will be substantially improved over the current state of the art.

Acknowledgments: The work at MIT was performed under the following financial assistance award 60NANB15D361 from U.S. Department of Commerce, National Institute of Standards and Technology.

Author Contributions: Daniel S. Hussey, Han Wen, Boris Khaykovich conceived and designed the experiments; Daniel S. Hussey, Boris Khaykovich, Thomas R. Gentile, Wangchun Chen, David L. Jacobson, Jacob M. LaManna performed the experiments; Daniel S. Hussey and Huarui Wu analyzed the data; Daniel S. Hussey and Boris Khaykovich wrote the paper.

Conflicts of Interest: The authors declare no conflict of interest.

References and Note

1. Eskildsen, M.R.; Gammel, P.L.; Isaacs, E.D.; Detlefs, C.; Mortensen, K.; Bishop, D.J. Compound refractive optics for the imaging and focusing of low-energy neutrons. *Nature* **1998**, *391*, 563–566.
2. Kardjilov, N.; Manke, I.; Strobl, M.; Hilger, A.; Treimer, W.; Meissner, M.; Krist, T.; Banhart, J. Three-dimensional imaging of magnetic fields with polarized neutrons. *Nat. Phys.* **2008**, *4*, 399–403. [[CrossRef](#)]
3. Treimer, W.; Ebrahimi, O.; Karakas, N.; Prozorov, R. Polarized neutron imaging and three-dimensional calculation of magnetic flux trapping in bulk of superconductors. *Phys. Rev. B* **2012**, *85*, 184522. [[CrossRef](#)]
4. Treimer, W. Radiography and tomography with polarized neutrons. *J. Magn. Magn. Mater.* **2014**, *350*, 188–198. [[CrossRef](#)]
5. Miao, H.; Panna, A.; Gomella, A.A.; Bennett, E.E.; Znati, S.; Chen, L.; Wen, H. A universal moiré effect and application in X-ray phase-contrast imaging. *Nat. Phys.* **2016**, *12*, 830–834. [[CrossRef](#)] [[PubMed](#)]
6. Pushin, D.A.; Sarenac, D.; Hussey, D.S.; Miao, H.; Arif, M.; Cory, D.G.; Huber, M.G.; Jacobson, D.L.; LaManna, J.M.; Parker, J.D.; et al. Far-field interference of a neutron white beam and the applications to noninvasive phase-contrast imaging. *Phys. Rev. A* **2017**, *95*, 043637. [[CrossRef](#)]
7. Khaykovich, B.; Gubarev, M.V.; Bagdasarova, Y.; Ramsey, B.D.; Moncton, D.E. From X-ray telescopes to neutron scattering: Using axisymmetric mirrors to focus a neutron beam. *Nucl. Instrum. Methods Phys. Res. Sect. A Accel. Spectrom. Detect. Assoc. Equip.* **2011**, *631*, 98–104. [[CrossRef](#)]
8. Liu, D.; Hussey, D.; Gubarev, M.V.; Ramsey, B.D.; Jacobson, D.; Arif, M.; Moncton, D.E.; Khaykovich, B. Demonstration of Achromatic Cold-Neutron Microscope Utilizing Axisymmetric Focusing Mirrors. *Appl. Phys. Lett.* **2013**, *102*, 183508. [[CrossRef](#)]
9. Hussey, D.S.; Brocker, C.; Cook, J.C.; Jacobson, D.L.; Gentile, T.R.; Chen, W.C.; Baltic, E.; Baxter, D.V.; Duskow, J.; Arif, M. A New Cold Neutron Imaging Instrument at NIST. *Phys. Procedia* **2015**, *69*, 48–54. [[CrossRef](#)]
10. Certain trade names and company products are mentioned in the text or identified in an illustration in order to adequately specify the experimental procedure and equipment used. In no case does such identification imply recommendation or endorsement by the National Institute of Standards and Technology, nor does it imply that the products are necessarily the best available for the purpose.
11. Gentile, T.R.; Babcock, E.; Borchers, J.A.; Chen, W.C.; Hussey, D.; Jones, G.L.; Lee, W.T.; Majkzrak, C.F.; O'Donovan, K.V.; Snow, W.M.; et al. Polarized spin filters in neutron scattering. *Phys. B Condens. Matter.* **2005**, *356*, 96–102. [[CrossRef](#)]
12. Chen, W.C.; Gentile, T.R.; Erwin, R.; Watson, S.; Ye, Q.; Krycka, K.L.; Maranville, B.B. ³He spin filter based polarized neutron capability at the NIST Center for Neutron Research. *J. Phys. Conf. Ser.* **2014**, *528*, 012014. [[CrossRef](#)]
13. Wen, H.; Bennett, E.E.; Hegedus, M.M.; Carroll, S.C. Spatial Harmonic Imaging of X-ray Scattering—Initial Results. *IEEE Trans. Med. Imaging* **2008**, *27*, 997–1002. [[CrossRef](#)] [[PubMed](#)]
14. Lefmann, K.; Nielsen, K. McStas, a general software package for neutron ray-tracing simulations. *Neutron News.* **1999**, *10*, 20–23. [[CrossRef](#)]
15. Willendrup, P.; Farhi, E.; Lefmann, K. McStas 1.7—A new version of the flexible Monte Carlo neutron scattering package. *Phys. B Condens. Matter.* **2004**, *350*, E735–E737. [[CrossRef](#)]
16. Wu, H.; Khaykovich, B.; Wang, X.; Hussey, D.S. Wolter mirrors for neutron imaging. *Phys. Procedia* **2017**, *88*, 184–189. [[CrossRef](#)]

